

Supporting Information

Incipient Microphase Separation in Short Chain Perfluoropolyether-*block*-Poly(ethylene oxide) Copolymers

Mahati Chintapalli^{a,b}, *Ksenia Timachova*^{b,c}, *Kevin R. Olson*^d, *Michał Banaszak*^e, *Jacob L. Thelen*^{c,f}, *Sue J. Meham*^d, *Joseph M. DeSimone*^{d,g}, *Nitash P. Balsara*^{*b,c,f}

Wide angle X-ray scattering of PFPE polymers

In Figure S1, WAXS profiles are shown for various PFPE polymers, at temperatures between 30 °C and 90 °C. The profiles in Figure S1a and S1b, for PFPE_{D10}-Diol and PFPE_{D10}-DMC, are qualitatively similar to each other, whereas the profiles in Figure S1c, for PFPE_{E10}-DMC, are qualitatively similar to those in Figure 1b for PFPE_{E10}-Diol.

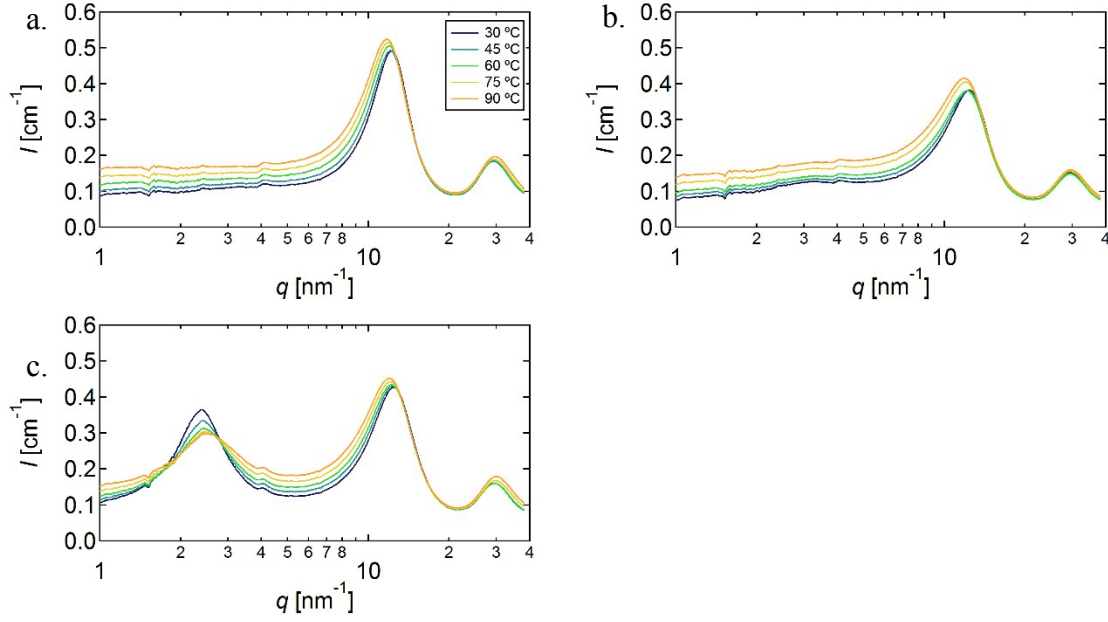


Figure S1. WAXS profiles as a function of temperature for PFPE polymers. In (a-c) WAXS profiles are shown for PFPE_{D10}-Diol, PFPE_{D10}-DMC, and PFPE_{E10}-DMC, respectively.

Structure Factors

The RPA structure factor is calculated for an ABA triblock of the sequence $f_1-f_2-f_3$, an ABABA pentablock of the sequence $f_1-f_2-f_3-f_4-f_5$, an ABABABA heptablock of the sequence $f_1-f_2-f_3-f_4-f_5-f_6-f_7$, and an ABABABABA nonablock of the sequence $f_1-f_2-f_3-f_4-f_5-f_6-f_7-f_8-f_9$. Here, f_n represents the volume fraction of a specific block in the sequence. For a polymer consisting of k coupled chains ($k=1$ is the uncoupled ABA triblock), the individual block fractions can be related to the overall volume fraction of the B block, ϕ_{PFPE} , according to the following equations.

$$f_n = \frac{1 - \phi_{PFPE}}{2k} \quad \text{for terminal A blocks } (n = 1 \text{ or } k) \quad (1)$$

$$f_n = \frac{1 - \phi_{PFPE}}{k} \quad \text{for internal A blocks } (\text{odd } n, \text{ and } n \neq 1 \text{ or } k) \quad (2)$$

$$f_B = \frac{\Phi_{PFPE}}{k} \quad \text{for B blocks, (even } n) \quad (3)$$

The following relationships (equations 4-13) are valid for all of the multiblocks ($k \geq 1$):

$$S(q) = g_{AA}(x) + 2g_{AB}(x) + g_{BB}(x) \quad (4)$$

$$W(q) = g_{AA}(x)g_{BB}(x) - [g_{AB}(x)]^2 \quad (5)$$

$$g_{AB}(x) = g_{BA}(x) \quad (6)$$

$$x \equiv q^2 R_{g,1}^2 \quad (7)$$

$$g^0(x) = \exp(-x) \quad (8)$$

$$g^1(x) = \frac{1 - \exp(-x)}{x} \quad (9)$$

$$g^2(x) = \frac{2(x + \exp(-x) - 1)}{x^2} \quad (10)$$

In equations 11-19, n is the number labelling the specific block in the sequence.

$$g_{n,n}(x) = f_n^2 g^2(f_n x) \quad (11)$$

$$g_{n,n+1}(x) = f_n f_{n+1} g^1(f_n x) g^1(f_{n+1} x) \quad (12)$$

$$g_{n,n+2}(x) = f_n f_{n+1} f_{n+2} g^1(f_n x) g^0(f_{n+1} x) g^1(f_{n+2} x) \quad (13)$$

In addition to the equations above, equations 14-15 are used for calculation of the pentablock and larger chains ($k \geq 2$):

$$g_{n,n+3}(x) = f_n[f_{n+1} + f_{n+2}]f_{n+3}g^1(f_n x)g^0([f_{n+1} + f_{n+2}]x)g^1(f_{n+3}x) \quad (14)$$

$$g_{n,n+4}(x) = f_n[f_{n+1} + f_{n+2} + f_{n+3}]f_{n+4}g^1(f_n x)g^0([f_{n+1} + f_{n+2} + f_{n+3}]x)g^1(f_{n+4}x) \quad (15)$$

Equations 16-17 are used for calculation of the heptablock and larger chains ($k \geq 3$).

$$g_{n,n+5}(x) = f_n[f_{n+1} + f_{n+2} + f_{n+3} + f_{n+4}]f_{n+5} g^1(f_n x) g^0([f_{n+1} + f_{n+2} + f_{n+3} + f_{n+4}]x) \\ \times g^1(f_{n+5}x) \quad (16)$$

$$g_{n,n+6}(x) = f_n[f_{n+1} + f_{n+2} + f_{n+3} + f_{n+4} + f_{n+5}]f_{n+6} g^1(f_n x) \\ \times g^0([f_{n+1} + f_{n+2} + f_{n+3} + f_{n+4} + f_{n+5}]x) \times g^1(f_{n+6}x) \quad (17)$$

Equations 18-19 are used for calculation of the nonablock ($k = 4$).

$$g_{n,n+7}(x) = f_n[f_{n+1} + f_{n+2} + f_{n+3} + f_{n+4} + f_{n+5} + f_{n+6}]f_{n+7} g^1(f_n x) \\ \times g^0([f_{n+1} + f_{n+2} + f_{n+3} + f_{n+4} + f_{n+5} + f_{n+6}]x) \times g^1(f_{n+7}x) \quad (18)$$

$$g_{n,n+8}(x) = f_n[f_{n+1} + f_{n+2} + f_{n+3} + f_{n+4} + f_{n+5} + f_{n+6} + f_{n+7}]f_{n+8} g^1(f_n x) \\ \times g^0([f_{n+1} + f_{n+2} + f_{n+3} + f_{n+4} + f_{n+5} + f_{n+6} + f_{n+7}]x) \times g^1(f_{n+8}x) \quad (19)$$

For the triblock ($k=1$), the equations 20-22 are used to calculate the terms $g_{AA}(x)$, $g_{BB}(x)$, and $g_{AB}(x)$. The commas in the subscripts on the right hand side of the equations are removed.

$$g_{AA}(x) = g_{11}(x) + g_{33}(x) + 2g_{13}(x) \quad (20)$$

$$g_{BB}(x) = g_{22}(x) \quad (21)$$

$$g_{AB}(x) = g_{12}(x) + g_{23}(x) \quad (22)$$

For the pentablock ($k=2$), equations 23-25 are used to calculate the terms $g_{AA}(x)$, $g_{BB}(x)$, and $g_{AB}(x)$.

$$g_{AA}(x) = g_{11}(x) + g_{33}(x) + g_{55}(x) + 2g_{13}(x) + 2g_{15}(x) + 2g_{35}(x) \quad (23)$$

$$g_{BB}(x) = g_{22}(x) + g_{44}(x) + 2g_{24}(x) \quad (24)$$

$$g_{AB}(x) = g_{12}(x) + g_{14}(x) + g_{23}(x) + g_{25}(x) + g_{34}(x) + g_{45}(x) \quad (25)$$

For the heptablock ($k=3$), equations 26-28 are used to calculate the terms $g_{AA}(x)$, $g_{BB}(x)$, and $g_{AB}(x)$.

$$g_{AA}(x) = g_{11}(x) + g_{33}(x) + g_{55}(x) + g_{77}(x) + 2g_{13}(x) + 2g_{15}(x) + 2g_{17}(x) + 2g_{35}(x) + 2g_{37}(x) + 2g_{57}(x) \quad (26)$$

$$g_{BB}(x) = g_{22}(x) + g_{44}(x) + g_{66}(x) + 2g_{24}(x) + 2g_{26}(x) + 2g_{46}(x) \quad (27)$$

$$\begin{aligned} g_{AB}(x) &= g_{12}(x) + g_{14}(x) + g_{16}(x) + g_{23}(x) + g_{25}(x) + g_{27}(x) + g_{34}(x) + g_{36}(x) + g_{45}(x) + g_{47}(x) + g_{56}(x) \\ &\quad + g_{67}(x) \end{aligned} \quad (28)$$

For the nonablock ($k=3$), equations 29-31 are used to calculate the terms $g_{AA}(x)$, $g_{BB}(x)$, and $g_{AB}(x)$.

$$\begin{aligned} g_{AA}(x) &= g_{11}(x) + g_{33}(x) + g_{55}(x) + g_{77}(x) + g_{99}(x) + 2g_{13}(x) + 2g_{15}(x) + 2g_{17}(x) + 2g_{19}(x) + 2g_{35}(x) \\ &\quad + 2g_{37}(x) + 2g_{39}(x) + 2g_{57}(x) + 2g_{59}(x) + 2g_{79}(x) \end{aligned} \quad (29)$$

$$g_{BB}(x) = g_{22}(x) + g_{44}(x) + g_{66}(x) + g_{88}(x) + 2g_{24}(x) + 2g_{26}(x) + 2g_{28}(x) + 2g_{46}(x) + 2g_{48}(x) + 2g_{68}(x) \quad (30)$$

$$\begin{aligned}
g_{AB}(x) &= g_{12}(x) + g_{14}(x) + g_{16}(x) + g_{18}(x) + g_{23}(x) + g_{25}(x) + g_{27}(x) + g_{29}(x) + g_{34}(x) + g_{36}(x) + g_{38}(x) \\
&+ g_{45}(x) + g_{47}(x) + g_{49}(x) + g_{56}(x) + g_{58}(x) + g_{67}(x) + g_{69}(x) + g_{78}(x) + g_{89}(x)
\end{aligned}
\tag{31}$$

Two Parameter Fits

In Figure S2, the values for radius of gyration, $R_{g,1}$, and Flory-Huggins interaction parameter, χ , are given as a function of temperature, determined from a two parameter fit to the RPA model. In this fit, the theoretical value was used for the contrast term, $c_{th} = 0.17 \text{ cm}^{-1}$. Qualitatively and quantitatively, the values are in good agreement with the values determined from the three parameter fits (Figure 4). Fits of the form $\chi = A + B/T$ are shown in Figure S2b. Because the value of c is fixed, the temperature dependence of χ is stronger in Figure S2b than in Figure 4b.

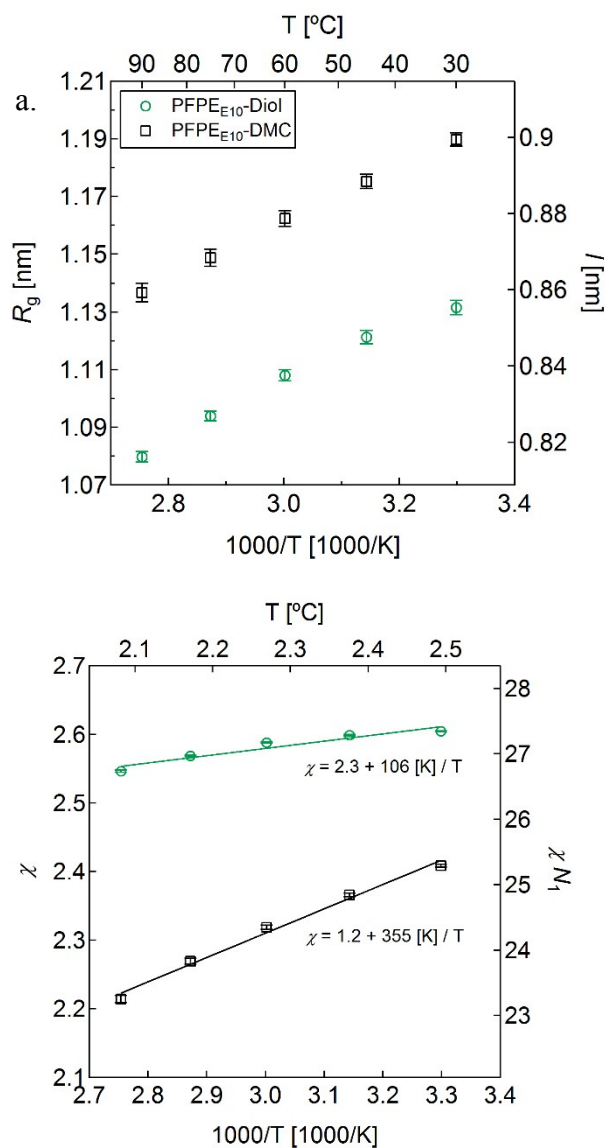


Figure S2. Random phase approximation parameters using a two-parameter fit. In (a), the radius of gyration, $R_{g,1}$, is given as a function of temperature, and in (b), the Flory-Huggins interaction parameter, χ , is given as a function of temperature. Fits of the form $\chi = A + B / T$ are shown.

Background Fit Parameters

The adjustable parameters in the background scattering function, a_0 , a_1 , and a_2 , are given in Figures S3 and S4. In Figure S3, the background parameters are given for the fit based on the variable c RPA model, and in Figure S4, the background parameters are given for the fit based on

the fixed c RPA model. The parameter a_0 represents the constant, temperature-dependent offset in scattering intensity, and the parameters a_1 and a_2 are from the Lorentzian function.

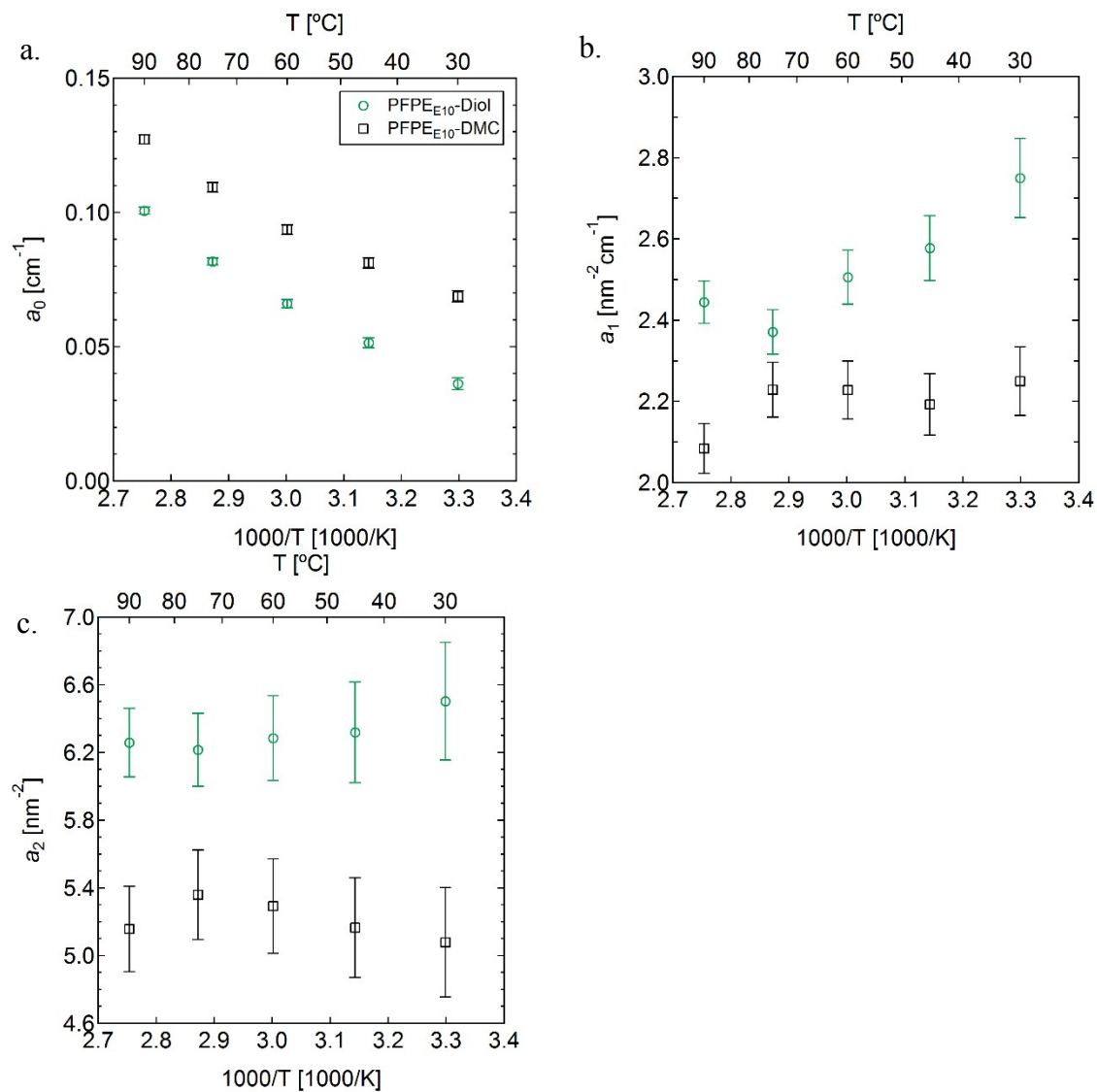


Figure S3. Background fit parameters for the RPA model with variable contrast, c . The values of the parameters a_0 , a_1 , and a_2 are given in (a), (b), and (c). Error bars represent the fit uncertainty.

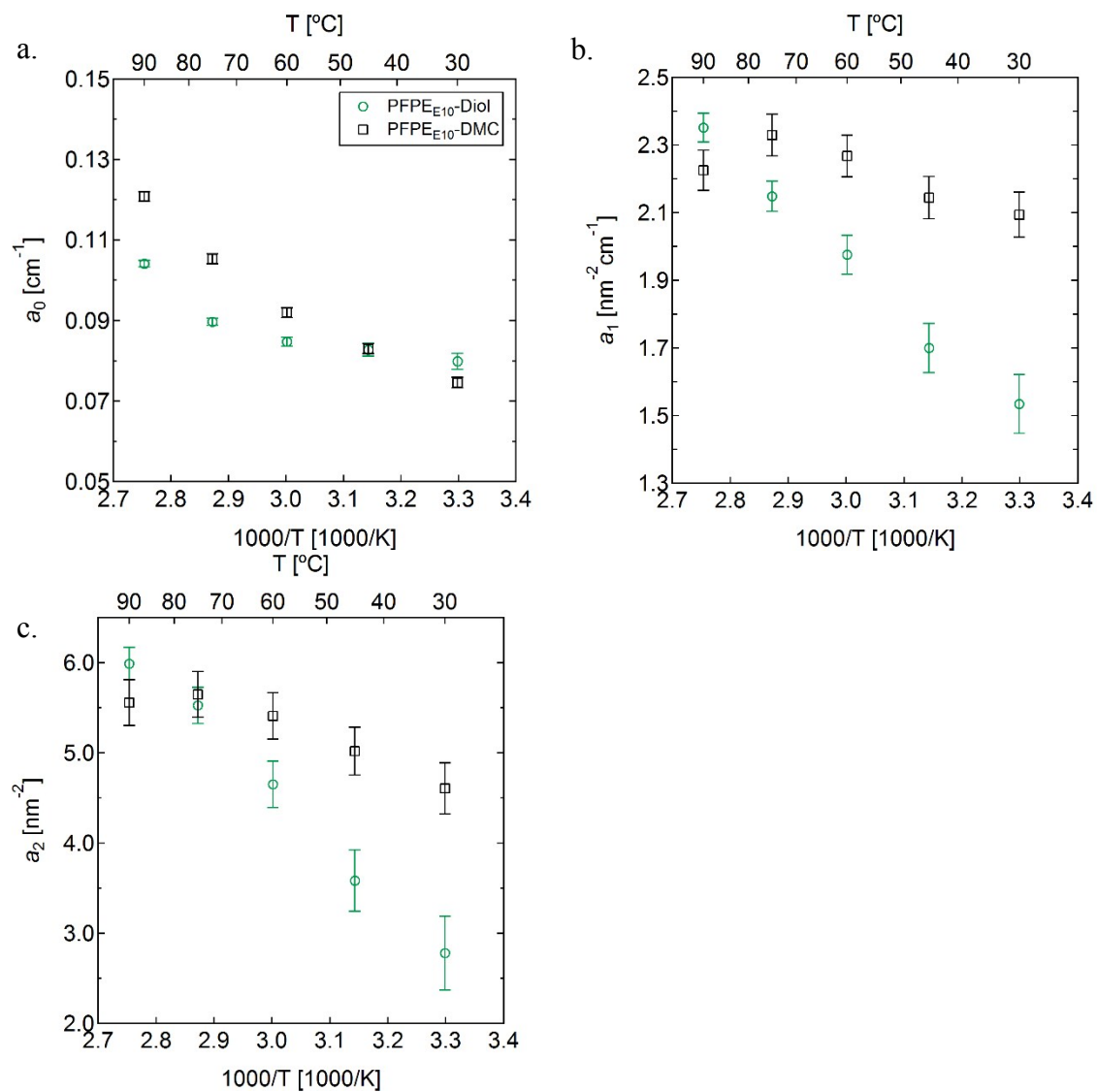


Figure S4. Background fit parameters for the RPA model with fixed contrast, c . The values of the parameters a_0 , a_1 , and a_2 are given in (a), (b), and (c). Error bars represent the fit uncertainty.